

Electronic Supplementary Information

Construction of Steady-Active Self-supported Porous Ir-based Electrocatalysts for Oxygen Evolution Reaction

Chemicals.

Ethanol (AR., Aladdin), borane tert-butylamine complex (BTB, 98%, Aladdin), commercial iridium oxide (99.9 %, Aladdin), cyclohexane (99.5%, Aladdin), dibenzyl ether (95%, Aladdin), dodecyl trimethyl ammonium bromide (DTAB, 99%, Aladdin), ethylene glycol (99%, Aladdin), ethylene Pyrrolidone (PVP, Aladdin), hexadecanediol (98%, Aladdin), iridium acetylacetonate (99.95%, Aladdin), iron acetylacetonate (98%, Aladdin), Nafion (5%, Aladdin), n-hexane (AR., Aladdin), oleic acid (AR., Aladdin), oleylamine (OAm, 80%~90%, Aladdin), perchloric acid (AR., Aladdin), Vulcan XC-72R (Aladdin). The water used in all experiments was deionized (18.2 M Ω ·cm). All the reagents were used as received without further purification.

Synthesis of Ir nanoparticles (NPs).

40 mg of Ir(acac)₃ and 10 mL of OAm were mixed into a three-necked flask and heated to 150 °C for 10 mins under a N₂ atmosphere. Then, 3 mL of OAm containing 200 mg of BTB were injected, and the solution was heated to 240 °C and kept at the temperature for 60 mins. After cooling to room temperature, ethanol was added to the solution to obtain Ir NPs precipitates. The product was washed with a mixture of hexane and ethanol several times and dissolved in hexane for further use.

Synthesis of Fe₃O₄ NPs.

25 mL of dibenzyl ether, 2 mL of oleylamine, and 2 mL of oleic acid were added to a three-necked flask and heated to 90 °C for 30 min in vacuum. Then, the solution was cooled to room temperature and added with a mixture of 2.3 g of hexadecanediol and 0.7063 g of iron acetylacetonate. After that, the solution was heated up to different temperatures for various times successively under a N₂ atmosphere (i.e., 120 °C for 60 min, 210 °C for 120 min, and 280 °C for 60 min). After cooling to room temperature, the Fe₃O₄ NP product was collected by adding ethanol and centrifuging.

Preparation of Spherical Assemblies.

65 mg of DTAB was dissolved in 5 mL of water to form a solution, and the hexane solution containing the NP mixture ($M_{\text{Ir}} : M_{\text{Fe}} \approx 1:1$) was added to the solution. The solution was stirred to form the microemulsion, heated to 50 °C, and kept at the temperature for 2 hours. 10 mL of ethylene glycol containing 1.1 g of PVP was added

to the evaporated solution, shake for 10 min, heated to 80 °C under the protection of nitrogen, and kept at the temperature for 6 hours. The assemblies were finally acquired by centrifugation.

Preparation of carbon-supported catalysts

40 mg of carbon powder in cyclohexane was dispersed in hexane and sonicated for 10 min. A catalyst-contained n-hexane solution was added and sonicated for 30 min. The solid was obtained by filtration and dried at 60 °C for 2 hours. The dried catalyst was annealed in the air at 300 °C for 5 hours to remove the surfactants.

X-ray Photoelectron Spectroscopy (XPS) Measurements

The XPS spectra were recorded on a Thermo Fisher ESCALAB 250Xi XPS system with a monochromatic Al K α X-ray source. The binding energies derived from XPS measurements were calibrated to the C 1s at 284.8 eV. The obtained spectra were fitted using XPS PEAK41. The major contributions and corresponding satellites were considered to fit the Ir4f region: the peaks at 61.0 and 64.0 eV were attributed to metallic Ir, those at 61.8 and 64.8 eV were assigned to Ir(IV) species and those at 62.4 and 65.4 eV were ascribed to Ir(III) species, those fitting at 63.1 and 66.1 eV were attributed to Ir(III) satellites, Ir 5p $_{1/2}$ and Ir(V) species give distinct contributions and an energy region at ca. 64 and ca. 67 eV were assigned to Ir(IV) satellites. The doublet separation between Ir 4f $_{7/2}$ and Ir 4f $_{5/2}$ was considered to be 3.0 eV and the height ratio between Ir 4f $_{7/2}$ and Ir 4f $_{5/2}$ peaks was 0.75. The results of the above peak fitting refer to the works of F. Claudel et al.^[1] and S. J. Freakley et al.^[2], respectively.

Physical Characterizations.

The XRD patterns were obtained on a Rigaku D/Max 2500 VB2+/PC X-ray powder diffractometer equipped with Cu K α radiation ($\lambda = 0.154$ nm) operating at 40 kV and 40 mA. The diffraction data were collected at a scanning rate of 10° min $^{-1}$. The TEM images were conducted by a HITACHI HT7700 transmission electron microscope. The elemental composition of Ir was detected by an inductively coupled plasma optical emission spectrometer (ICP-OES, Optima 7300 DV). The HRTEM image, EDS mapping, and EDS face scanning were performed on a JEOL JEM-2010F transmission electron microscopy. The elemental leaching amounts of Ir were detected

by an inductively coupled plasma mass spectrometry (ICP-MS, Agilent 7700). The contact angle tests were shot by a high-speed CCD camera (X-Motion, AOS Technologies). The specific surface area was determined using Brunauer-Emmett-Teller (BET) analysis and pore size distributions was calculated by performing Barret-Joyner-Halenda (BJH) analysis using the desorption branch of the isotherms.

Electrochemical tests.

The electrochemical performance of the catalysts was tested using a conventional three-electrode system. The reference electrode is a saturated calomel electrode (SCE), the counter electrode is a carbon rod, and the surface of the working electrode is coated with catalyst. For the preparation of the working electrodes, the as-prepared sample (containing 5 mg of carbon-supported nanocatalysts) was dispersed in 1000 μL of mixed solution (985 μL of isopropanol and 15 μL of Nafion (5 wt %)). Then the ink was sonicated into homogeneous dispersion. Then, 15 μL of the as-obtained ink was dropped onto a glassy carbon electrode to cover an area of 0.19625 cm^{-2} , resulting in the catalyst loading of $0.375\text{ mg}\cdot\text{cm}^{-2}$. Electrochemical measurements were performed on a CHI 760E potentiostat (CH Instruments, Inc., Shanghai, China), the electrolyte was 0.1 M HClO_4 solution, the rotation speed was 1600 rpm, and the scan rate was $50\text{ mV}\cdot\text{s}^{-1}$ or $5\text{ mV}\cdot\text{s}^{-1}$. At the same time, it is necessary to ensure that oxygen in the electrolyte is saturated.

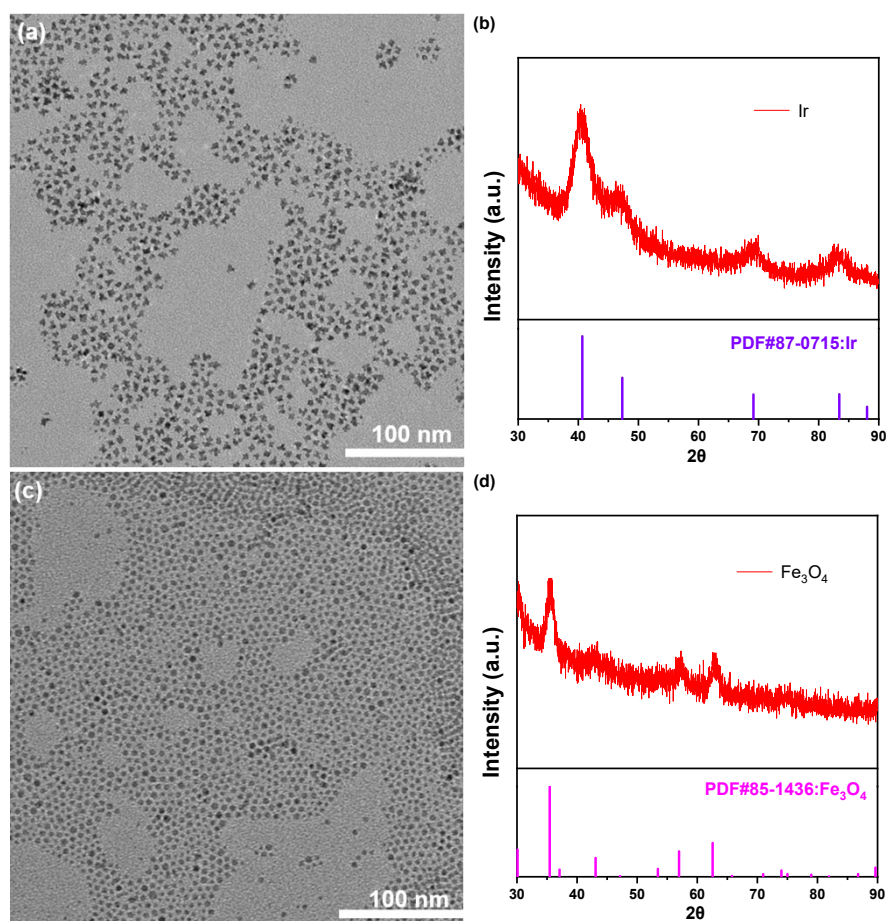


Figure S1. (a) The TEM image and (b) the XRD pattern of the Ir NPs; (c) The TEM image and (d) the XRD pattern of the Fe₃O₄ NPs.

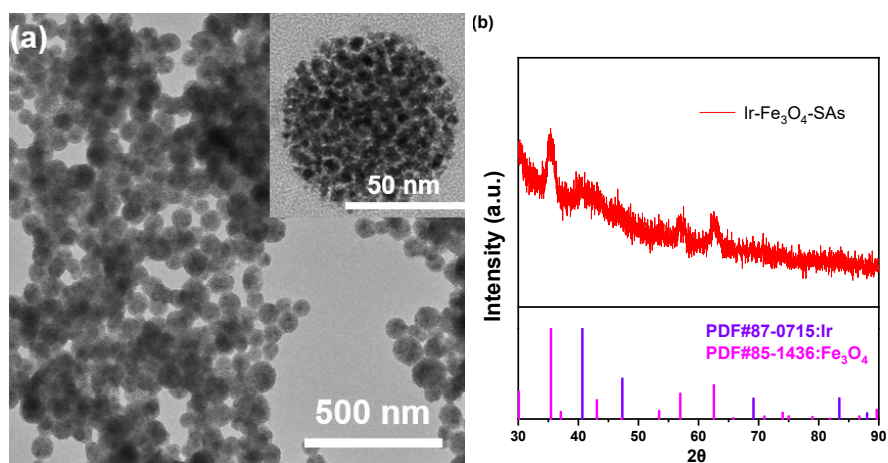


Figure S2. (a) The TEM image and (b) the XRD pattern of the Ir-Fe₃O₄-SAs. The inset is the enlarged TEM image.

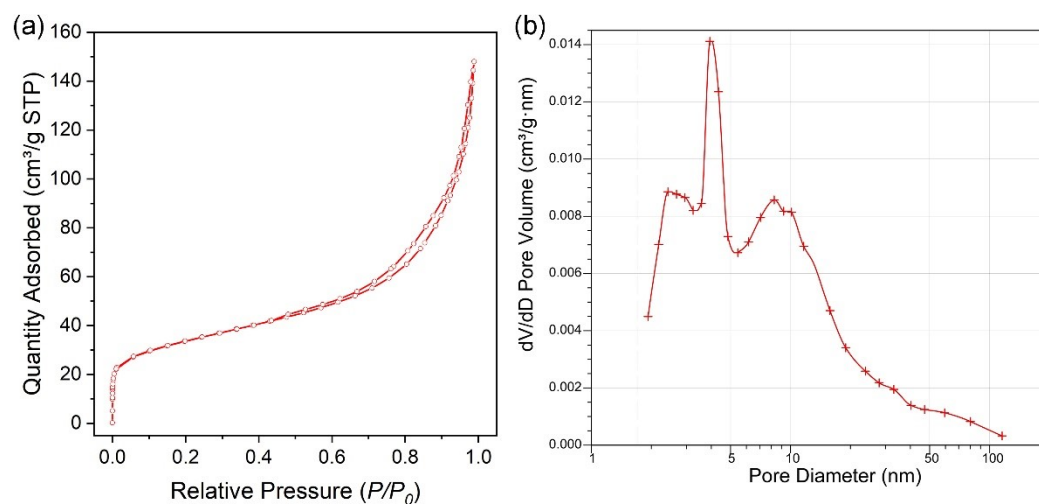


Figure S3. (a) The N₂ ad/desorption isotherm, and (b) the pore size distribution of the p-Ir-SAs (no carbon support). The pores at 2-3 nm and 10 nm might be attributed to the interparticle space and the cavity of the assemblies, respectively.

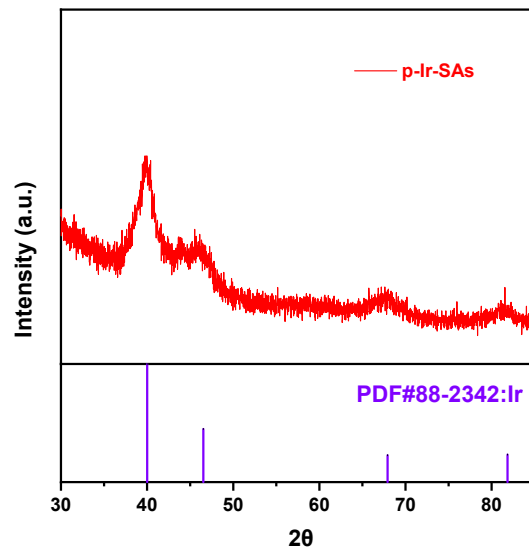


Figure S4. The XRD patterns of the p-Ir-SAs.

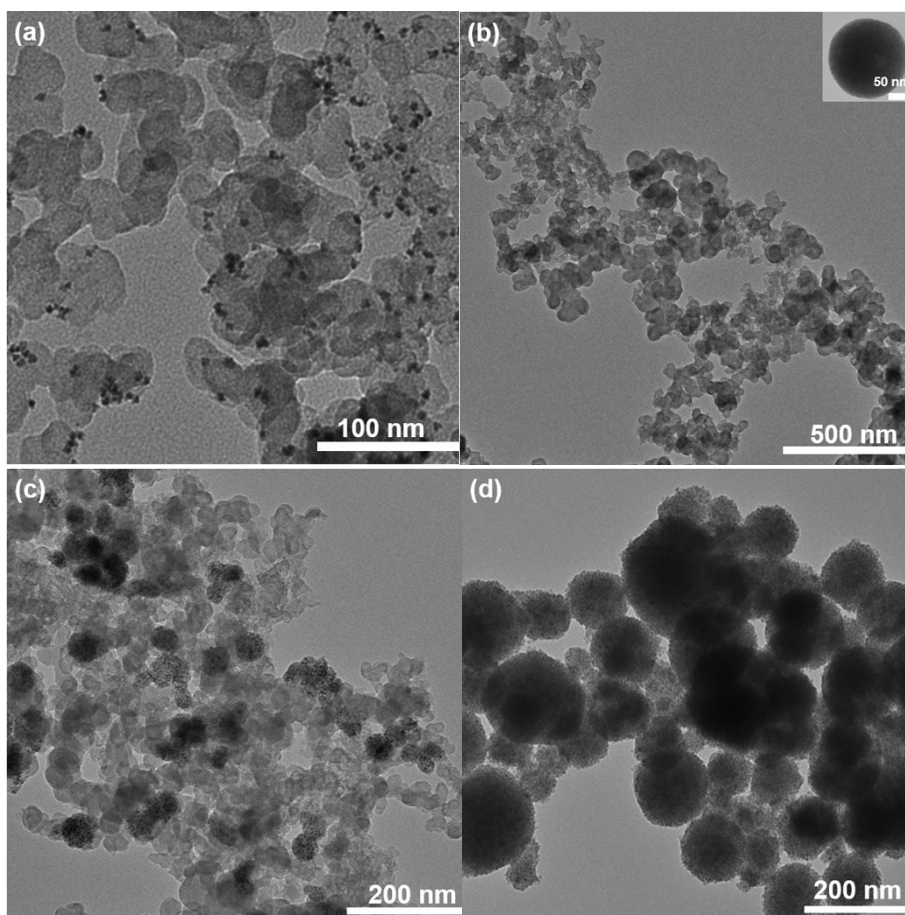


Figure S5. The TEM images of the (a) Ir/C, (b) Ir- SAs/C, (c) Ir- Fe₃O₄-SAs/C, and (d) Fe₃O₄-SAs/C.

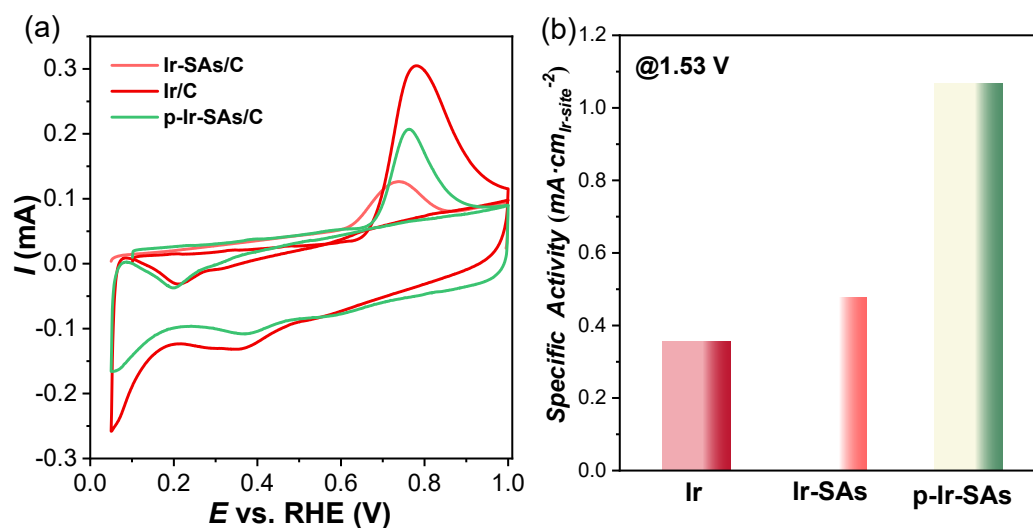


Figure S6. (a) The CO-stripping voltammograms, and (b) the normalized specific activity of Ir/C, Ir-SAs/C, and p-Ir-SAs/C. Electrolyte: 0.1M HClO_4 aqueous solution; test temperature: 30 °C; scan rate: 10 mV/s.

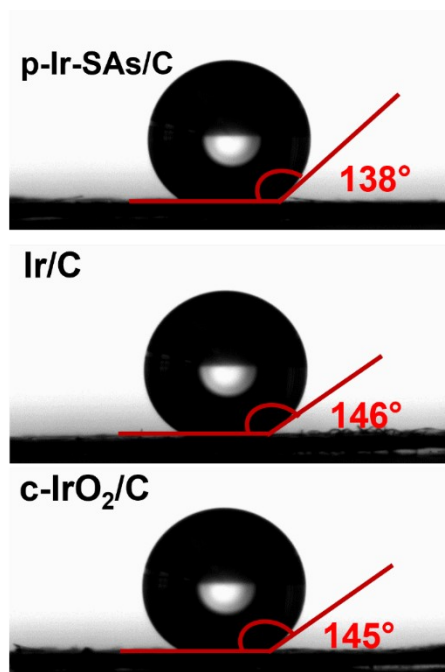


Figure S7. The contact angle tests of Ir/C, p-Ir-SAs/C, and c-IrO₂/C. Typically, a hydrophilic surface shows a low liquid contact angle and can yield a rapid expulsion of gas, beneficial to the mass transfer of gas evolution reactions.

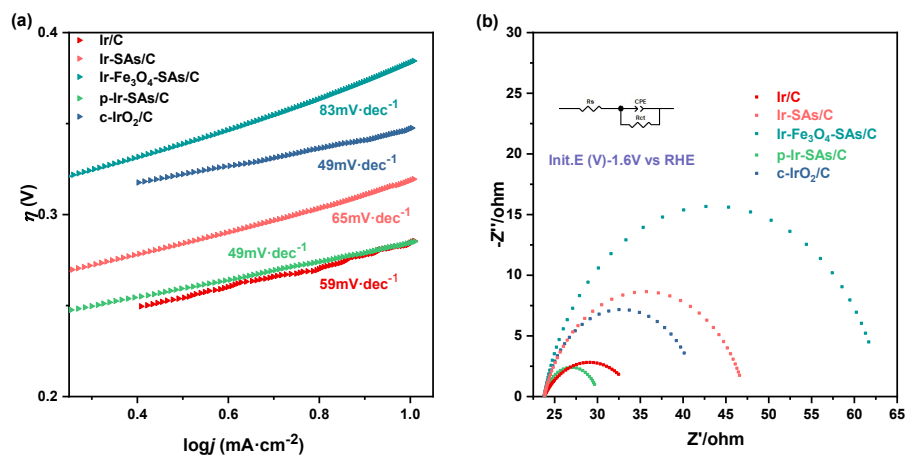


Figure S8. (a) The Tafel plots and (b) the Nyquist plots of Ir/C, Ir-SAs/C, Ir-Fe₃O₄-SAs/C, p-Ir-SAs/C, c-IrO₂/C. All the samples showed similar internal resistances of 24 Ω , suggesting similar test conditions.

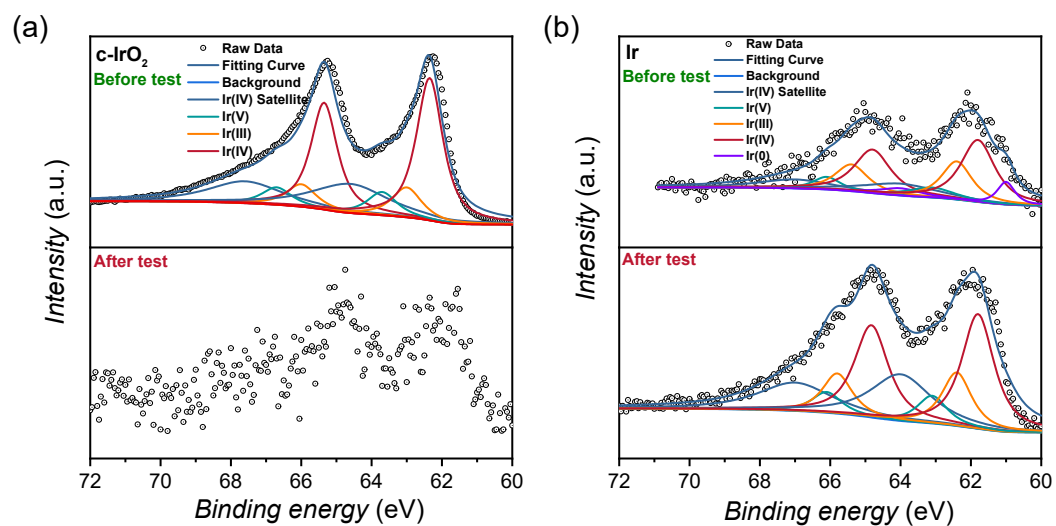


Figure S9. The high-resolution core-level Ir 4f XPS spectra before and after the AST for (a) the c-IrO₂/C and (b) the Ir/C.

Table S1. Contents of the synthesized iridium-based catalysts determined by ICP-OES in weight percentages.

	Contents(Ir)	Contents(Fe)	Ir-Loading
Ir/C	15.2%	/	57 ug/cm ²
Ir-SAs/C	13.1%	/	49 ug/cm ²
Ir- Fe ₃ O ₄ -SAs/C	2.0%	/	7.5ug/cm ²
p-Ir-SAs/C	10.3%	0.9%	37.5 ug/cm ²
c-IrO ₂ /C	20%	/	75 ug/cm ²

Table S2. Summary of OER activities of the synthesized Ir-based catalysts.

catalysts	ECSA (cm ²)	j_s @1.53 V (mA cm ⁻²)	j_m @1.53V(A g _{Ir} ⁻¹)	Tafel slope (mV dec ⁻¹)	η_{10}
Ir/C	9.07	0.36	278	59	284
Ir-SAs/C	2.37	0.48	115	65	319
Ir- Fe ₃ O ₄ -SAs/C	/	/	107.6	83	387
p-Ir-SAs/C	4.00	1.07	554	49	284
c-IrO ₂ /C	/	/	14.7	49	347

Table S3. Comparison of OER activities of the Ir-based catalysts reported in the literature.

Catalyst	Loading ($\mu\text{gIr cm}^{-2}$)	Electrolyte	η (mV) @ 10 mA cm^{-2}	η (mV) @ 50 mA cm^{-2}	Mass activity ($\text{A g}_{\text{Ir/PGM}}^{-1}$)	Ref.
Ir/Fe ₄ N	76.5	0.5 M H ₂ SO ₄	316	/	120 @1.54 V	[3]
IrO _x -Ir	133	0.5 M H ₂ SO ₄	295	/	8 @1.48V	[4]
Ir _{0.7} Ni _{0.3} O _x	102	0.5 M H ₂ SO ₄	340	440	198@1.6V	[5]
TiN/IrO ₂	79	0.5 M H ₂ SO ₄	313	350	874@1.6 V	[6]
IrNiCu	20	0.1 M HClO ₄	303	/	460 @1.53 V	[7]
DNF Ir film	/	0.1 M HClO ₄	293	/	39@1.525 V	[8]
Ir-Ni bulk	/	0.1 M HClO ₄	300	/	325@1.525 V	[9]
p-Ir-SAs	37.5	0.1 M HClO ₄	284	326	554@1.53 V	This work

Table S4 The XPS fitting parameters and results of the Ir 4f spectra for all the tested samples before and after the ASTs.

Peak Assignment	B.E. (eV)*	Content (p-Ir-SAs before)	Content (p-Ir-SAs after)	Content (Ir before)	Content (Ir after)	Content (c-IrO ₂ before)	Content (c-IrO ₂ after)
Ir 4f7/2	61.0						
Ir(0)		4%	0%	10%	0%	0%	NA
Ir 4f5/2	64.0						
Ir(0)							
Ir 4f7/2	61.8						
Ir(IV)	(62.3)	61%	38%	51%	67%	71%	NA
Ir 4f5/2	64.8						
Ir(IV)	(65.3)						
Ir 4f7/2	62.4						
Ir(III)	(63.0)	28%	44%	28%	21%	16%	NA
Ir 4f5/2	65.4						
Ir(III)	(66.0)						
Ir 4f7/2	63.1						
Ir(V)	(63.7)	7%	18%	11%	12%	13%	NA
Ir 4f5/2	66.1						
Ir(V)	(66.7)						

*The binding energies in the parentheses are the fitting values for the c-IrO₂/C. The values shifted 0.6 eV to the high B.E. as compared with the other two catalysts due to the high oxidation status.

Reference

- S1 F. Claudel, L. Dubau, G. Berthomé, L. Sola-Hernandez, C. Beauger, L. Piccolo and F. Maillard, *ACS Catal.*, **2019**, 9, 4688-4698.
- S2 S. J. Freakley, J. Ruiz-Esquisus and D. J. Morgan, *Surf. Interface Anal.*, **2017**, 49, 794-799.
- S3 B. M. Tackett, W. Sheng, S. Kattel, S. Yao, B. Yan, K. A. Kuttiyiel, Q. Wu and J. G. Chen, *ACS Catal.*, **2018**, 8, 2615-2621.
- S4 P. Lettenmeier, L. Wang, U. Golla-Schindler, P. Gazdzicki, N. A. Cañas, M. Handl, R. Hiesgen, S. S. Hosseiny, A. S. Gago and K. A. Friedrich, *Angew. Chem. Int. Ed.*, **2016**, 55, 742-746.
- S5 S. Xu, S. Chen, L. Tian, Q. Xia and W. Hu, *J Solid State Electrochem*, **2016**, 20, 1961-1970.
- S6 K. Zhang, W. Mai, J. Li, H. Wang, G. Li and W. Hu, *J. Mater. Sci.*, **2020**, 55, 3507-3520.
- S7 J. Park, Y. J. Sa, H. Baik, T. Kwon, S. H. Joo and K. Lee, *ACS Nano*, **2017**, 11, 5500-5509.
- S8 C. Spöri, P. Briois, H. N. Nong, T. Reier, A. Billard, S. Köhl, D. Teschner and P. Strasser, *ACS Catal.*, **2019**, 9, 6653-6663.
- S9 T. Reier, Z. Pawolek, S. Cherevko, M. Bruns, T. Jones, D. Teschner, S. r. Selve, A. Bergmann, H. N. Nong and R. Schlögl, *J. Am. Chem. Soc.*, **2015**, 137, 13031-13040.